PHILOSOPHICAL TRANSACTIONS OF THE ROYAL SOCIETY B BIOLOGICAL SCIENCES

Elementary Excitations in Liquid <latex>^{3}</latex>He

K. Skold and C. A. Pelizzari

Phil. Trans. R. Soc. Lond. B 1980 **290**, 605-616
doi: 10.1098/rstb.1980.0119

Phil. Trans. R. Soc. Lond. B **290**, 605–616 (1980)
Printed in Great Britain

Elementary excitations in liquid ^{3}He

By K. Sköld†‡ and C. A. Pelizzari‡
† *The Studsvik Science Research Laboratory, S-61182 Nyköping, Sweden*
‡ *Solid State Science Division, Argonne National Laboratory, Argonne, Illinois 60439, U.S.A.*

The two isotopes of helium offer unique opportunities to test fundamental theories of quantum fluids. In liquid ^{4}He, a Bose liquid, the elementary excitations have been studied extensively over the last two decades by neutron inelastic scattering. Similar studies of liquid ^{3}He, the Fermi liquid counterpart of liquid ^{4}He, have become possible only recently. From the results obtained so far for normal liquid ^{3}He, the existence of zero sound as a well defined density excitation at finite wavevectors ($q \approx q_F$) and finite temperatures ($T \approx T_F$) has been verified and the spin fluctuation spectrum has been measured. By comparing the neutron scattering results for the density fluctuation spectrum with R.P.A. calculations with generalized polarization potentials, important information has been obtained about the effective spin-symmetric interaction between ^{3}He atoms. The spin fluctuation spectrum is in agreement with the paramagnon model if a value close to unity is assumed for the contact dimensionless paramagnon parameter $\bar{I}$. This implies that the nuclear spin system in normal liquid ^{3}He is close to ferromagnetic.

Introduction

A wealth of information regarding the elementary excitation spectrum in liquid ^{4}He has been obtained from neutron inelastic scattering measurements over the past 20 years (Price 1978). Practically all the information that is now available about the density fluctuation spectrum on a microscopic level has been obtained from studies of this kind. In liquid ^{3}He it is only recently that such measurements have become possible. The reason for this is the large neutron absorption cross section of the ^{3}He nucleus, which renders neutron scattering experiments rather difficult in this system.

In order to specify completely the dynamics of liquid ^{3}He, it is necessary to determine both the dynamics of the atoms (density fluctuations) and of the nuclear spin system (spin fluctuations). It is a most fortunate circumstance that the neutron probe couples both to the density fluctuations and to the spin fluctuations. This is due to the fact that the neutron scattering amplitude of the ^{3}He nucleus is different for the singlet and the triplet scattering states. The neutron scattering function therefore contains two components, namely the spin fluctuation scattering and the density fluctuation scattering.

The first neutron scattering results for liquid ^{3}He are those reported by Scherm *et al.* (1974). More extensive results were later reported by Stirling *et al.* (1975, 1976). These measurements were all made at the high-flux reactor at Institut Laue–Langevin in Grenoble. The spectra observed by the Grenoble group show a broad peak of inelastically scattered neutrons around energy transfers corresponding to the excitation of single particle–hole pairs, i.e. single particle excitations of the kind expected for a Fermi fluid, plus a long tail at larger energies. No evidence of a collective density mode of the zero sound type, which was predicted over 10 years ago by

Pines (1966), was observed in these experiments. The lowest temperature of the Grenoble experiments was 0.63 K and spectra were recorded for wavevector transfers larger than about 1 Å^{-1}†. In a subsequent experiment by the present authors (Sköld *et al.* 1976), the neutron scattering function for liquid ^{3}He at 15 mK was measured for wavevectors in the range 0.8 Å^{-1} $\leqslant q \leqslant$ 2.2 Å^{-1}. These measurements were made at the CP-5 reactor at Argonne National Laboratory and the results show structure not observed in the Grenoble results. In particular, for $q \leqslant 1.3$ Å^{-1} the spectra display two peaks, namely one at *ca.* 0.2 meV and one at *ca.* 1 meV. The low energy peak is within the particle–hole band and is identified as spin-fluctuation scattering. The peak at *ca.* 1 meV is the zero sound mode predicted by Pines (1966). In a second experiment, the Argonne Group measured the scattering function for wavevectors down to 0.55 Å^{-1} (Sköld & Pelizzari 1977). In this case, dispersion of the zero sound mode is observed at the smaller wavevectors. In a recent experiment, the Argonne group has determined the scattering function at 40 mK and at 1.2 K and for wavevectors in the range 0.4 Å^{-1} $\leqslant q \leqslant$ 2.2 Å^{-1} (Sköld & Pelizzari 1978*a*). These experiments were designed to study the temperature dependence of the scattering function and, in particular, to elucidate the discrepancy of the results obtained by the Argonne group and those obtained by the Grenoble group. The results show that for $q \lesssim 1.2$ Å^{-1} and $T = 1.2$ K the zero sound mode is still a well defined excitation but that the spin fluctuation peak shows considerable broadening at the higher temperature. Thus, the discrepancy of the results obtained by the two groups can not be reconciled by the difference in the temperatures at which the results were obtained.

In the present report the results obtained by the Argonne group are discussed in some detail. The neutron scattering results are compared with theoretical predictions obtained from R.P.A. calculations with generalized polarization potentials in the density fluctuation spectrum and with the predictions of the paramagnon model in the spin fluctuation spectrum. It is shown that the density fluctuation spectrum can be fitted with the R.P.A. results if q-dependent effective interactions and a q-dependent effective mass is assumed. The experimental results for the spin fluctuation spectrum are in good agreement with the paramagnon model with the paramagnon parameter close to 1, i.e. the nuclear spin system appears to be close to ferromagnetic.

Theoretical overview

The theoretical models considered in this paper all have the same basic structure, namely that of the R.P.A. theory. In this case the dynamical function of interest is the density–density (spin–spin) response function $\chi^{C,I}(q, E)$, where C labels the density function and I labels the spin function. The corresponding neutron scattering functions are related to the response functions by

$$S^{C,I}(q, E) = -\pi^{-1} \operatorname{Im} \chi^{C,I}(q, E). \tag{1}$$

In the R.P.A. theory the response function is expressed in terms of the screened response function, $\chi^{C,I}_{sc}(q, E)$, and the effective interaction, $\psi^{C,I}(q)$:

$$\chi^{C,I}(q, E) = \frac{\chi^{C,I}_{sc}(q, E)}{1 + \psi^{C,I}(q)\, \chi^{C,I}_{sc}(q, E)}. \tag{2}$$

The screened response function describes the response of the system to the sum of an applied external field and the polarization fields produced by the density (spin) fluctuations. The effective interaction measures the strength of the polarization fields.

† 1 Å = 10^{-10} m = 10^{-1} nm.

In the approach taken by Aldrich & Pines (1978), in addition to the scalar polarization field produced by density fluctuations, the vector polarization field produced by current fluctuations is also considered. The scalar interaction is derived from the Fourier transform of an assumed analytical form for the effective two-body potential in r-space:

$$f_q^{\mathrm{s}} = \frac{4\pi}{V}\int_0^\infty \mathrm{d}r\, r^2 \frac{\sin qr}{qr}\, \tfrac{1}{2}\{f^{\uparrow\uparrow}(r)+f^{\uparrow\downarrow}(r)\} \tag{3}$$

and

$$f_q^{\mathrm{a}} = \frac{4\pi}{V}\int_0^\infty \mathrm{d}r\, r^2 \frac{\sin qr}{qr}\, \tfrac{1}{2}\{f^{\uparrow\uparrow}(r)-f^{\uparrow\downarrow}(r)\}, \tag{4}$$

where $f^{\uparrow\uparrow}(r)$ ($f^{\uparrow\downarrow}(r)$) is the interaction between particles of parallel (antiparallel) spins. The spin symmetric (s) and the spin asymmetric (a) interactions apply to the density fluctuation and the spin fluctuation fields respectively. The repulsive part of the effective interaction is parametrized in the following form:

$$f^{\uparrow\uparrow}(r) = a^{\uparrow\uparrow}[1-(r/r_{\mathrm{c}}^{\uparrow\uparrow})^8] \qquad r \leqslant r_{\mathrm{c}}, \tag{5}$$

with a similar expression for the spin asymmetric interaction. For $r > r_{\mathrm{c}}$, an attractive van der Waals interaction is assumed. For f_q^{s} it is further postulated that

$$\tfrac{1}{2}\{f^{\uparrow\uparrow}(r)+f^{\downarrow\uparrow}(r)\} = a_{\mathrm{s}}[1-(r/r_{\mathrm{s}})^8] \quad r \leqslant r_{\mathrm{s}}, \tag{6}$$

i.e. the same functional form as in (5) is assumed. The value of a_{s} is determined by $f_q^{\mathrm{s}} = 0$ from the corresponding Landau parameter, while r_{s} is determined from a comparison with the experimental neutron scattering results. In the spin asymmetric interaction, we consider the effect of differences in $r_{\mathrm{c}}^{\uparrow\uparrow}$ and $r_{\mathrm{c}}^{\uparrow\downarrow}$ on $S^{\mathrm{I}}(q, E)$. Aldrich & Pines (1978) also include the vector interaction $(\omega/q)^2 g_q^{\mathrm{s}}$ in their description of the density fluctuation spectrum. The parameter g_q^{s} is related to the effective mass through

$$m_q^* = m_0 + N g_q^{\mathrm{s}}, \tag{7}$$

where m_0 is the bare ^{3}He mass and N is the number density. The effective mass parameter m_q^* (or g_q^{s}) is a phenomenological parameter in the theory and is adjusted to fit the neutron scattering data. Finally, to allow for multi particle–hole contributions to χ_{sc}, the one-particle χ_{sc} is renormalized according to

$$\omega_{\mathrm{sc}}^{\mathrm{C,I}}(q, E) = \alpha_q^{\mathrm{C,I}} \chi_0^*(q, E) + \chi_{\mathrm{m}}^{\mathrm{C,I}}(q, E), \tag{8}$$

where χ_0^* is the Lindhard response function with effective mass from (7), α_q is another phenomenological parameter and χ_{m} is approximated by

$$\chi_{\mathrm{m}}^{\mathrm{C,I}}(q, E) = \chi_{\mathrm{m}}^{\mathrm{C,I}}(q, 0). \tag{9}$$

The phenomenological constants that appear in the theory are chosen such that in the limit $q \to 0$ the Landau–Fermi liquid theory is recovered.

The R.P.A. results with the phenomenological interactions described above are compared with the neutron scattering results for the density fluctuation spectrum. As discussed by Aldrich & Pines (1978), the same approach can also be used to analyse the spin fluctuation spectrum. In this case the effective interaction is due to subtle differences between the interaction of particles of parallel spins and the interaction of particles of antiparallel spins (compare equation (4)). It is observed that a difference of only 3 % in the range of the repulsive core could lead to a spin-wave instability at finite q.

PHILOSOPHICAL TRANSACTIONS OF THE ROYAL SOCIETY B BIOLOGICAL SCIENCES

In a recent publication by Beal-Monod (1979), the spin fluctuation spectrum is analysed within the framework of the R.P.A. theory but with the parameters chosen in accordance with the values appropriate to the paramagnon model (Doniach & Engelsberg 1966). In this case, the tendency to magnetic ordering is emphasized, the mass enhancement is neglected and the interaction is represented by the contact spin–spin repulsion parameter $\bar{I}$:

$$\chi^{\mathrm{I}}(q, E) = \chi_0(q, E)/\{1+\bar{I}\chi_0(q, E)\}, \tag{10}$$

where χ_0 is the Lindhard function for the bare mass. From the neutron scattering results published earlier by the present authors (Sköld *et al.* 1976), Beal-Monod obtains $\bar{I} \approx 0.9$. This is consistent with the experimentally observed enhancement in the static susceptibility. As $\bar{I} = 1$ is the Stoner criterion for a ferromagnetic instability, the results imply that normal liquid ^{3}He at low temperatures ($T \ll T_{\mathrm{F}}$) is nearly ferromagnetic. These conclusions are supported by the results presented in this paper in which recent and more extensive neutron scattering results are compared with the predictions of the paramagnon model.

Experimental arrangements

The experimental arrangements are described in detail by Sköld *et al.* (1980). In the present context a brief summary of the most important aspects will therefore suffice.

The experiments reported here present several difficulties not ordinarily encountered in neutron scattering measurements. Most importantly, the large ratio of the neutron absorption cross section and the neutron scattering cross section of the ^{3}He nucleus ($\sigma_{\mathrm{a}} \approx 11\,000$ b† at $\lambda_{\mathrm{n}} \approx 4$ Å; $\sigma_{\mathrm{s}} \approx 6$ b) severely limits the statistical accuracy of the experimental results. Also, the weak signal from the sample requires that the experimental arrangement be designed such that systematic errors are minimized as much as possible. To study the fully developed quantum statistical properties of a Fermi fluid the temperature should be well below the Fermi temperature. For liquid ^{3}He ($T_{\mathrm{F}}^* \approx 1.5$ K) this implies that the temperature of the measurement should be less than a few tenths of a kelvin and a dilution cryostat is therefore required.

The neutron scattering experiments were made at the TNTOFS spectrometer at the CP-5 reactor at Argonne National Laboratory (Kleb *et al.* 1973). The TNTOFS instrument is a time-of-flight spectrometer which can be used either with a conventional Fermi chopper or with a statistical chopper. The statistical chopper has a duty cycle of *ca.* 50 % and is in general superior to the conventional chopper in applications where the total background on the detector is larger than twice the total signal that is obtained when the conventional chopper is used (Sköld 1968*a*, *b*; Price & Sköld 1970). In the present experimental situation the background is two orders of magnitude larger than the signal for the conventional chopper and the statistical chopper therefore offers a significant advantage in this case.

The large absorption in the sample enhances the relative importance of extraneous scattering in the sample region, such as scattering from the sample container. With a strongly absorbing sample the only practical configuration is to scatter neutrons off the sample surface with the detectors in reflexion geometry. This arrangement is illustrated schematically in figure 1 for a container of conventional design and for the particular container used in the present studies. With sample in the container, neutrons are scattered in a thin layer at the surface of the sample

† 1 barn (b) = 10^{-28} m^2.

PHILOSOPHICAL TRANSACTIONS OF THE ROYAL SOCIETY B BIOLOGICAL SCIENCES

(the $1/e$ distance for 4 Å neutrons in liquid ^{3}He is *ca.* 0.05 mm) and also in the front wall of the container. The data must be corrected for the scattering in the front wall and this component is determined in a separate experiment in which the scattering from the empty container is measured. However, with the container empty, neutrons also strike the back wall of the container. For a container of conventional design, neutrons scattered off the back wall can reach the detectors. With the wedge-shaped container used in the present studies, neutrons striking the back wall cannot reach the detectors and the scattering from the front wall is in this case properly determined from a separate experiment with the container empty.

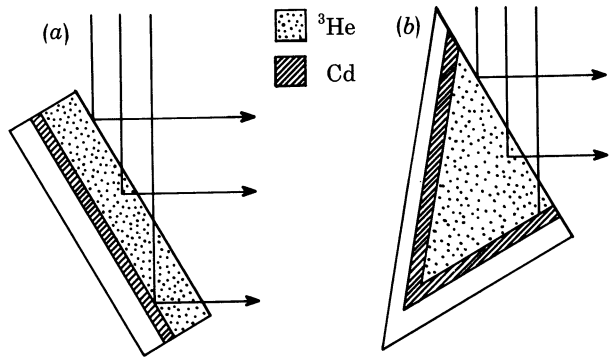

FIGURE 1. (*a*) Sample container of conventional design; (*b*) the particular design used in the present experiments.

The data must also be corrected for the energy dependent absorption in the sample. This correction is sensitive to the inclination of the sample surface to the incident and to the scattered neutron beams. As explained by Sköld *et al.* (1980), with a special device the orientation of the sample inside the cryostat is determined to within $\pm 0.25°$. To determine the scattering functions of an absolute scale, it is furthermore necessary to calibrate a number of spectrometer constants, such as the efficiencies of the beam monitors and of the detectors. This is accomplished by measuring the number of neutrons elastically scattered from a slab of vanadium into each detector for a given count on the beam monitors. The absolute normalization of the experimental scattering function is accurate to within *ca.* 10 %.

The scattering functions are determined for $T = 40$ mK and for $T = 1.2$ K and in each case time-of-flight spectra are recorded at 15 angles of scattering in the range 13.2–110.4°. The incident neutron energy is 4.94 meV and the energy resolution of the instrument varies from 0.25 meV at small angles of scattering to 0.30 meV at large angles of scattering.

EXPERIMENTAL RESULTS

By using standard correction procedures (Copley *et al.* 1973), the experimentally observed time-of-flight spectra are converted to scattering functions at constant angle of scattering. As explained above, the observed functions contain contributions both from the density fluctuation scattering and from the spin fluctuation scattering, weighted by their respective bound scattering cross sections

$$S(q, E) = S^{\mathrm{C}}(q, E) + (\sigma_{\mathrm{i}}/\sigma_{\mathrm{c}})\, S^{\mathrm{I}}(q, E), \tag{11}$$

where $\sigma_c = 4.9$ b is assumed for the coherent cross section (Kitchens *et al.* 1974); the value for the spin-dependent scattering cross section, σ_i, is discussed below. Examples of experimentally determined scattering functions at constant angles of scattering are shown in figure 2 for the two temperatures of the experiment. In the constant-angle representation, the value of the wavevector transfer varies with the energy transfer, and selected values of q are shown at the top of the graphs in figure 2.

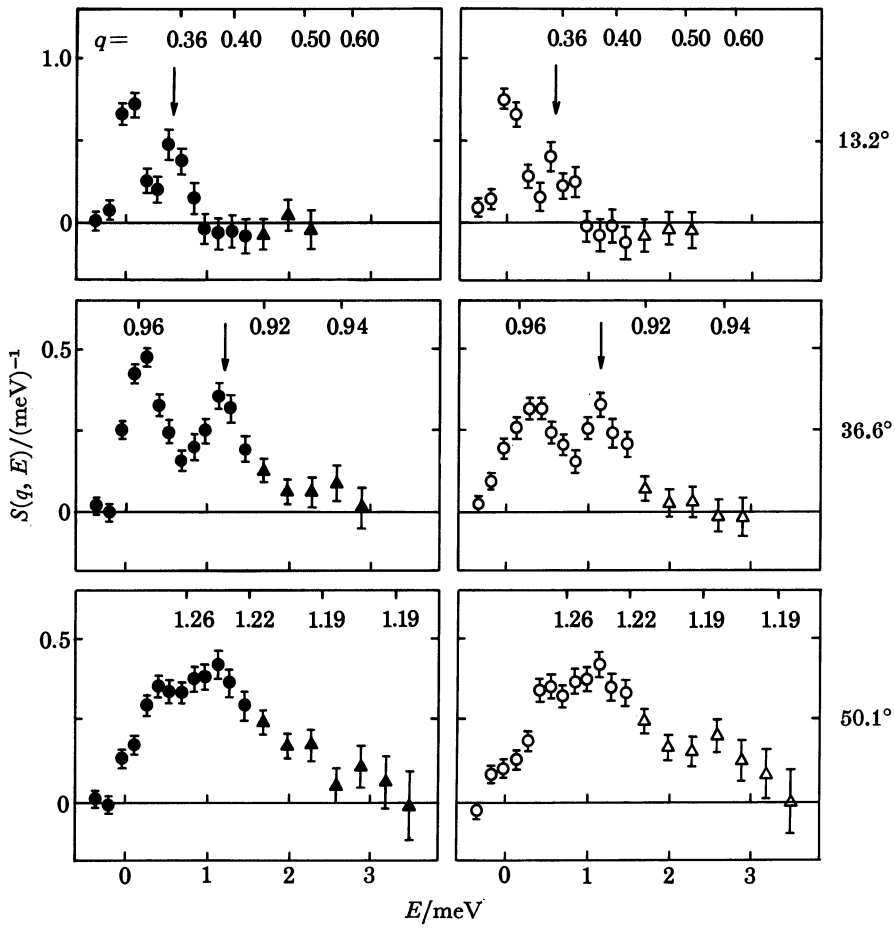

FIGURE 2. Selected examples of the scattering functions at constant value of the scattering angle. Data to the left are for $T = 40$ mK and data to the right are for $T = 1.2$ K. Vertical bars on the data points indicate the statistical uncertainty of the data points (± 1 standard deviation). Values of q are in reciprocal ångströms.

Analysis of the scattering functions in terms of theoretical models is best done at constant value of q, and such representations are presented and discussed below. It is useful, however, to identify important features in the results shown in figure 2, as these are more directly related to the actual observations. From the results shown in figure 2 the following general conclusions can be drawn. For small values of q the scattering functions show two peaks, one peak at *ca.* 0.1–0.2 meV, which is due to the excitation of particle–hole (p–h) pairs, and one peak at *ca.* 1 meV, which is the zero sound mode. For $q \gtrsim 1.3$ Å^{-1}, the two peaks merge, the zero sound mode approaches the upper edge of the p–h band and is Landau damped. The spectral weight of the tail at large energies, which is identified as multiple p–h excitations, increases with increasing q as expected. From the results shown in figure 2 it is clear that the zero sound

mode continues to be a well defined excitation at 1.2 K while the p–h peak shows considerable broadening at the higher temperature. The thermal broadening is clearly displayed in the middle graphs in figure 2. For the data shown in the top graphs in figure 2 the shape of the spin fluctuation spectrum is dominated by the instrumental resolution and the broadening with temperature is therefore not obvious in this case ($\Delta E_{\mathrm{res}} \approx 0.25$ meV).

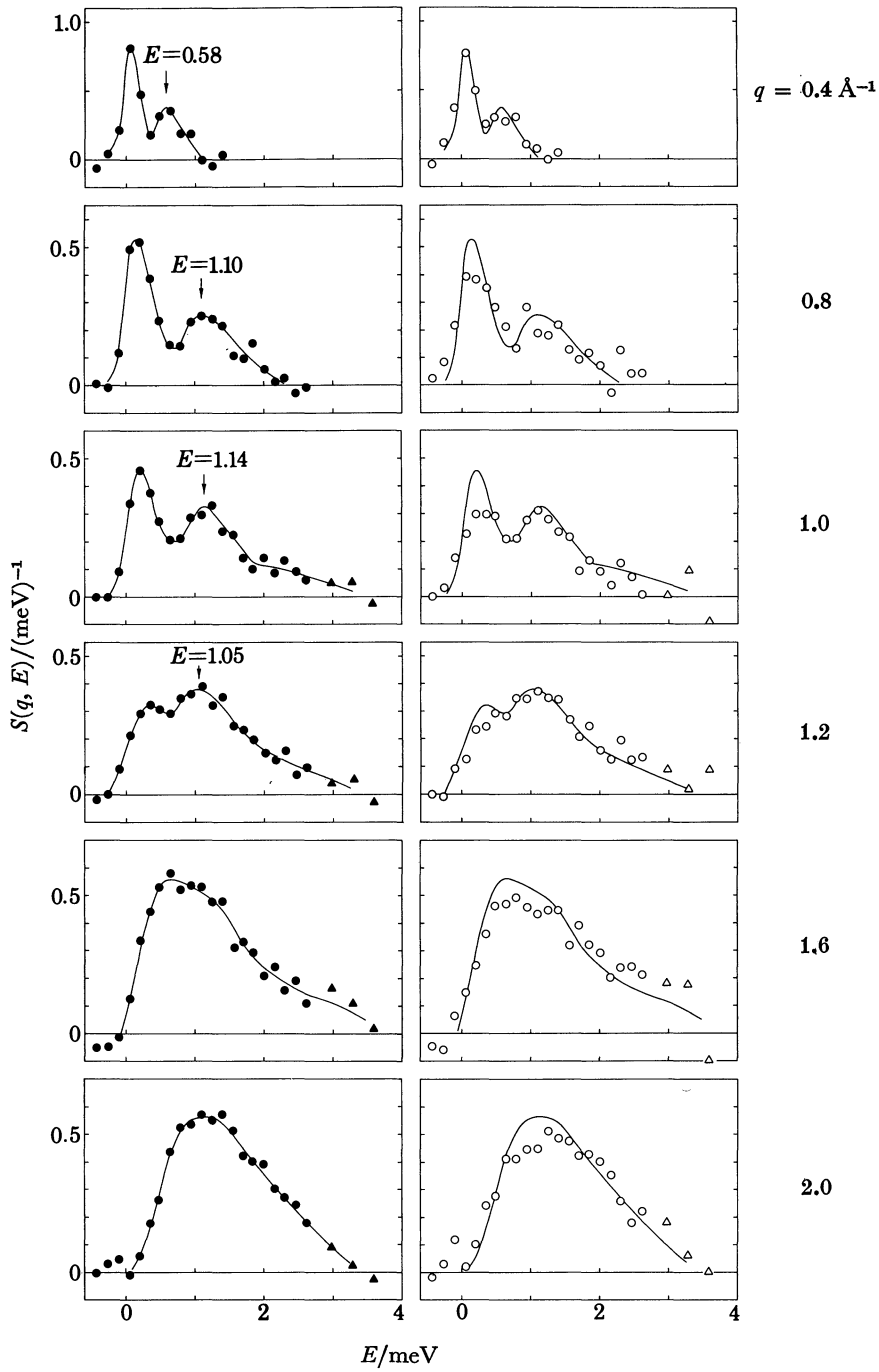

FIGURE 3. Selected examples of the scattering function at constant value of the scattering vector, q. The solid lines are fitted by eye to the results for $T = 40$ mK (left) and are also shown together with the results for 1.2 K (right).

To facilitate comparison with theoretical models, it is convenient to consider the scattering function at constant value of q rather than at constant angle of scattering. The constant q representation is derived by interpolation of the functions measured at constant angles of scattering. For each energy transfer, a cubic spline is fitted by least squares to the 15 constant-angle data points and the spline function is then used as a representation of the scattering function at arbitrary values of q. For a detailed account of the interpolation procedure, see Sköld *et al.* (1980). Examples of the constant q results are shown in figure 3. The solid curves in figure 3 are fitted by eye to the 40 mK data and are also shown with the 1.2 K data to demonstrate the change in the scattering function with temperature. The main features of the constant q curves are similar to those already observed in the constant-angle data, namely, for $q \lesssim 1.3$ Å^{-1} the scattering function shows two peaks plus a tail at large energies. The major difference between the data at 40 mK and at 1.2 K is the broadening observed in the particle–hole spectrum. The interpretation of the results in quantitative terms is discussed in the next section.

Theoretical interpretation

For detailed analysis of the experimental results we concentrate on the data for $T = 40$ mK. As noted above, the major difference between these results and those observed at 1.2 K is the broadening of the particle–hole spectrum at the higher temperature. For a discussion of finite temperature effects, see recent publications by Glyde & Khanna (1977, 1980) and Aldrich & Pines (1978).

To extract quantitative information from the experimental results, a phenomenological function has been fitted by least squares to the observed scattering function. The phenomenological function is the sum of three components, namely one function that describes the p–h spectrum, one that describes the zero sound peak and one that accounts for the multi-pair (m.p.) spectrum at large energies.

From a consideration of the Landau limit of the R.P.A. theory, it is easy to show that the spectral weight of the density fluctuation spectrum inside the p–h band is negligible at small values of q (Aldrich *et al.* 1976*a*). The p–h spectrum is therefore dominated by spin fluctuation scattering and in the fitting procedure it is assumed that this is the case at all values of q considered ($q \leqslant 1.3$ Å^{-1}). This component is represented by the paramagnon model (equation (10)) with $\bar{I}$ and the weight as fitting parameters. The theoretical function is folded with the resolution function before being compared to the experimental points. The zero sound peak is represented by a Gaussian function with position, width and area as parameters. The tail at large energies is fitted by a Gaussian centred at 2 meV, and with f.w.h.m. equal to 2 meV. As the statistical accuracy of the data at large energies is rather poor, the spectral weight of this component has been adjusted such that the f-sum rule is satisfied for the density fluctuation spectrum. The paramagnon model exhausts the f-sum rule for the spin spectrum and it is therefore assumed that there is no spin contribution to the m.p. spectrum.

The general conclusion is that the phenomenological model described above allows a very precise description of the experimental results; a typical example of the agreement achieved is shown in figure 4. However, the result shown in figure 4 indicates that the three components to the scattering function overlap to a substantial degree. This implies that the numerical results obtained for the individual components are strongly correlated. To assess the uniqueness of the results obtained from the model-fitting procedure, another model for the spin fluctuation

PHILOSOPHICAL TRANSACTIONS OF THE ROYAL SOCIETY B BIOLOGICAL SCIENCES

spectrum is therefore also considered. In this case the p–h band is fitted by the function appropriate to the non-interacting Fermi gas with $m_q^* = 3\,m_0$ and the spectral weight as the only fitting parameter. The results of this model are shown together with those obtained from the paramagnon model whenever appropriate. The results obtained from this analysis are summarized in figure 5. The energy of the zero sound mode is shown in figure 5*a*, together with the p–h band. The disappearance of the zero sound mode at $q \approx 1.3$ Å^{-1} is seen to be consistent with $m_q^* = 3\,m_0$. Landau damping (decay of the mode into p–h excitations) will act to damp the

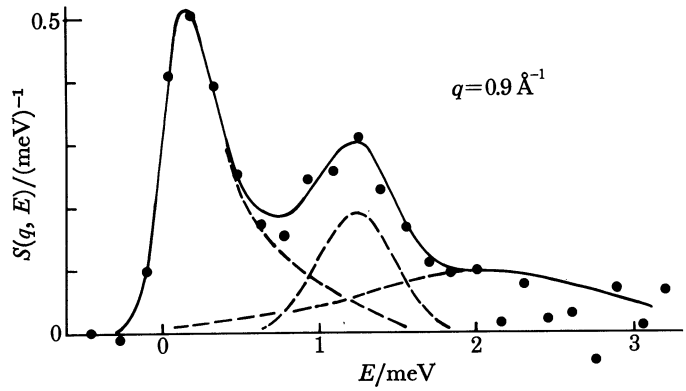

FIGURE 4. Example of the fit of the phenomenological function to the experimental scattering function as explained in the text. The solid line shows the sum of the component functions (broken curves).

mode very efficiently as the mode approaches the band edge and the position of the band edge is determined by m_q^*. The theoretical curve shown in figure 5*a* is the result obtained by Aldrich & Pines (1978) and is adjusted to fit the curve shown by the open circles, which were the only results available at that time. Although the present analysis of the experimental results suggests a need to re-evaluate the parameters in the R.P.A. model it is of interest to discuss the implications of the theoretical fit. The R.P.A. results are based on $r_c^{\uparrow\uparrow} = r_c^{\uparrow\downarrow} = 3.0$ Å, which should be compared with the value 2.68 Å which these authors obtain from a similar analysis of the excitation spectrum of liquid ^{4}He (Aldrich & Pines 1976; Aldrich *et al.* 1976*b*). They speculated that the difference between liquid ^{3}He and liquid ^{4}He is due to more effective short-range screening of the bare interaction in the case of liquid ^{3}He, which has a much larger zero point amplitude. Aldrich & Pines (1978) suggest that an experiment on liquid ^{3}He at elevated pressure, such that the zero point amplitude is reduced to a value comparable to that in liquid ^{4}He at s.v.p., may help to verify this hypothesis. Such experiments have been attempted (Hilton *et al.* 1978; Sköld & Pelizzari 1978*b*) but so far results that are accurate enough to be useful in this regard have not been obtained. The pressure dependence of the zero sound mode has also been discussed recently by Glyde & Khanna (1980).

Figure 5*b* shows the spectral weight of the zero sound mode. As in the case of the mode energy, these results are also rather sensitive to the assumed shape of the p–h spectrum. However, the overall shape of the curves are rather similar in the two cases and in general agreement with calculations (Aldrich 1974). The sharp rise in the curve at *ca.* 1.2 Å^{-1} signifies the strong coupling to p–h excitations as the mode approaches the band edge.

The results for the width of the mode, shown in figure 5*c*, are perhaps more surprising. The increase for $q \gtrsim 1.2$ Å^{-1} is expected and is due to the onset of Landau damping. However, the local increase in the width for $q \approx 0.6$ Å^{-1} is a novel feature, not predicted by any of the

PHILOSOPHICAL TRANSACTIONS OF THE ROYAL SOCIETY B BIOLOGICAL SCIENCES

theoretical models currently available. We believe that this phenomenon can be explained if reference is made to the dispersion curve shown in figure 5*a*, namely, the zero sound mode shows large positive dispersion in the range $0.5\ \text{Å}^{-1} \lesssim q \lesssim 0.8\ \text{Å}^{-1}$ and decay of the mode into two excitations of lower q, and E is then kinematically allowed. This process has already been considered for liquid ^{4}He where the positive dispersion is much less pronounced than that observed here. However, in view of the large uncertainties in the present results and in the absence of detailed calculations it is not meaningful to discuss this hypothesis quantitatively; it is therefore left as a qualitative conjecture at this time. The width of the zero sound mode at other values of q could be explained by damping through decay into multipair excitations. This process is not included in the R.P.A. calculations discussed above, as these calculations use screened response functions corresponding to single excitations only. Decay of the zero sound mode due to multipair interaction has, however, been considered by Glyde & Khanna (1980). Using the theory for sound propagation in a dilute Fermi gas that includes scattering of quasi-particles, they calculate that the width of the collective mode is 0.22 meV at $q = 0.5\ \text{Å}^{-1}$ and 0.35 meV at $q = 1.0\ \text{Å}^{-1}$. Assuming, as above, that the peak in the width curve at $q \approx 0.6\ \text{Å}^{-1}$ is due to multiphonon decay and that the increase in the width for $q \gtrsim 1.2\ \text{Å}^{-1}$ is due to Landau damping, the results obtained by Glyde & Khanna for the multipair damping are entirely consistent with the results shown by the solid circles in figure 5*c*. Note that the experimental results shown in figure 5*c* are corrected for resolution broadening and thus represent the true line width of the mode. It should also be noted that the overlap of the p–h band with the zero sound mode, such as shown in figure 4, does not suggest a damping mechanism as, for reasons of symmetry, single particle spin fluctuations do not couple to the density mode.

Figure 5*d* shows the area of the m.p. spectrum. With the assumptions made above, the total fitted function fulfils the *f*-sum rule. It is gratifying to note that the function is in very good agreement with the data (compare figure 4). This implies that the absolute normalization of the data is rather accurate. For small values of q the spectral weight of the m.p. spectrum should vary as q^4. The results shown in figure 5*d* are approximately consistent with this behaviour at all values of q.

The result for the spin fluctuation spectrum are shown in figure 5*e*, which shows the values obtained for the paramagnon parameter, $\bar{I}$, and for the weight function, σ_i/σ_c. For consistency the value of σ_i/σ_c should be the same at all values of q. The present results yield $\sigma_i/\sigma_c = 0.2 \pm 0.05$ for the average value. This is consistent with the result obtained previously from a direct determination of the spin structure factor, namely $\sigma_i/\sigma_c = 0.25$ (Sköld *et al.* 1976). The value for $\bar{I}$ is in the range 0.9–1.0, which should be compared with $\bar{I} = 0.895$, the value obtained from the enhancement in the static susceptibility, and to $I \approx 0.9$, the value obtained by Beal-Monod (1979) from an analysis of earlier neutron scattering data by the present authors. Within the accuracy of the methods used to extract $\bar{I}$ from the experimental scattering function, these results are all consistent and support the view that normal liquid ^{3}He is nearly ferromagnetic. It would be of considerable interest to extend the neutron scattering measurements to lower values of q and to improve the energy resolution such that the intrinsic shape of the spin fluctuation spectrum is resolved. This would allow a more definite comparison of the neutron scattering results to the predictions of the paramagnon model. It would also be of considerable interest to study the spin fluctuation spectrum at elevated pressure and to search for indications of a magnetic instability in the nuclear spin system at finite q, as discussed by Aldrich & Pines (1978).

PHILOSOPHICAL TRANSACTIONS OF THE ROYAL SOCIETY B BIOLOGICAL SCIENCES

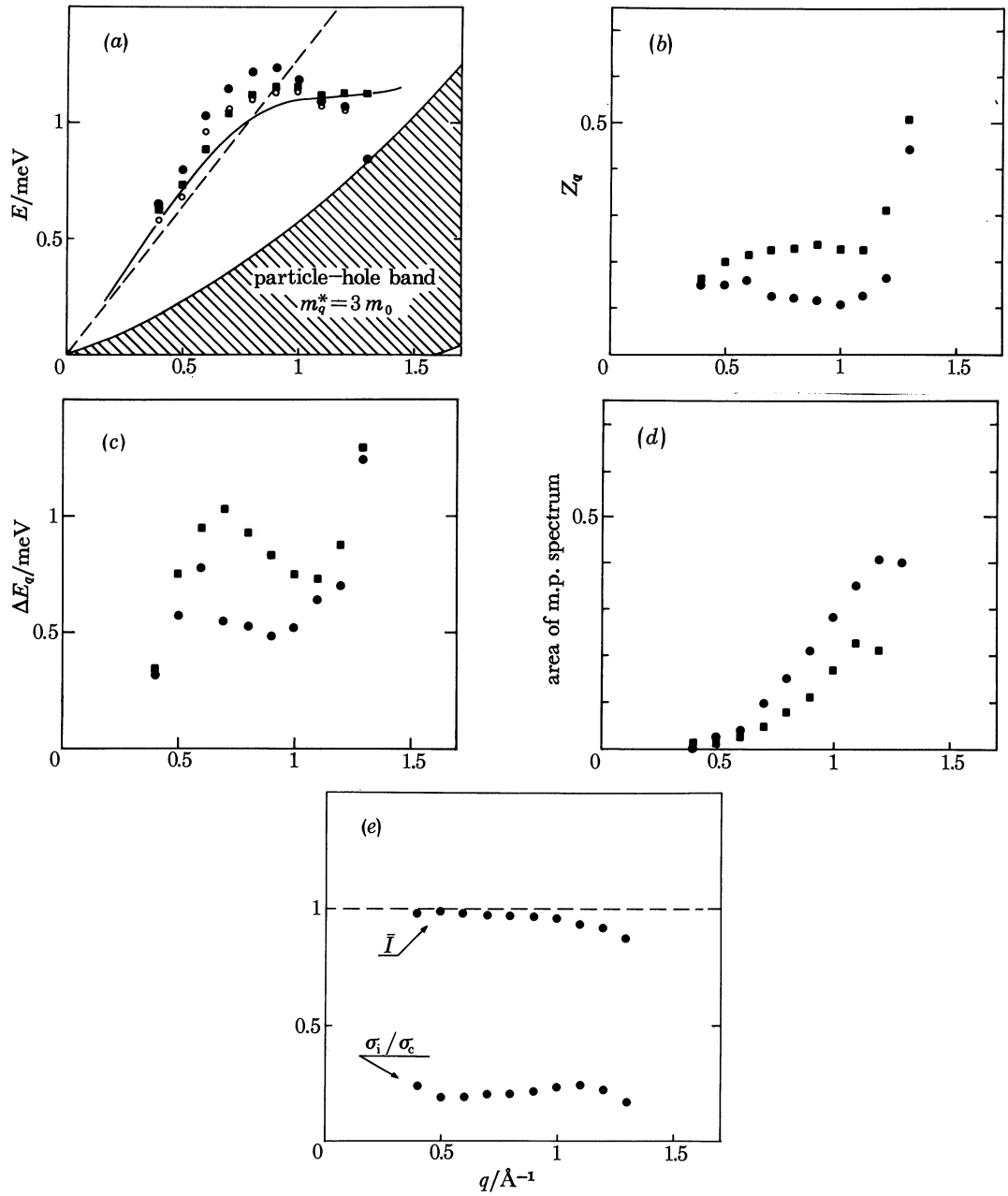

FIGURE 5. Parameters of the phenomenological function fitted to the experimental neutron scattering function for $T = 40$ mK. (*a*) Energy of the zero sound mode if the spin fluctuation peak is fitted by the paramagnon model (●) and if the spin fluctuation peak is fitted by the free Fermi gas model (■). Open circles show the results obtained if the peak positions are estimated by eye. (*b*) Spectral weight of the zero sound mode. Symbols as above. (*c*) Full width at half maximum of the zero sound mode. Symbols as above. (*d*) Area of the multi-pair spectrum. Symbols as above. (*e*) Parameters of the paramagnon model.

DISCUSSION

The results discussed in this paper demonstrate that the neutron scattering results now available for liquid ^{3}He are accurate enough to allow very detailed comparison to theoretical models. From a phenomenological decomposition of the scattering function, useful information about both the spin fluctuation spectrum and the density fluctuation spectrum is obtained.

PHILOSOPHICAL TRANSACTIONS OF THE ROYAL SOCIETY B BIOLOGICAL SCIENCES

The width of the collective density mode shows a complex behaviour as a function of the wavevector transfer. The results suggest that decay into single pair and multipair excitations as well as phonon–phonon decay may be important damping processes. The spin fluctuation spectrum is analysed in terms of the paramagnon model and a value for the paramagnon parameter close to unity is deduced.

For the future, it is suggested that measurements at elevated pressure would be of considerable interest. In the density fluctuation spectrum a variation of the average density would elucidate the importance of the zero point amplitude for the local screening of the effective repulsive pair interaction. In the spin fluctuation spectrum a variation of the density may lead to an enhancement in the spin-asymmetric interaction and, possibly, to a magnetic instability at finite q. It would also be of considerable interest to study the spin fluctuation spectrum with improved energy resolution such that the intrinsic shape of the paramagnon peak at small q is resolved. This would allow a detailed examination of the spin contribution to the effective pair interaction.

References (Sköld & Pelizzari)

Aldrich III, C. H. 1974 Ph.D. thesis, University of Illinois.
Aldrich III, C. H. & Pines, D. 1976 *J. low Temp. Phys.* **25**, 677–690.
Aldrich III, C. H. & Pines, D. 1978 *J. low Temp. Phys.* **32**, 698–715.
Aldrich III, C. H., Pethick, C. J. & Pines, D. 1976*a* *Phys. Rev. Lett.* **37**, 845–848.
Aldrich III, C. H., Pethick, C. J. & Pines, D. 1976*b* *J. low Temp. Phys.* **25**, 691–697.
Beal-Monod, M. T. 1979 *J. low Temp. Phys.* **37**, 123–134.
Copley, J. R. D., Price, D. L. & Rowe, J. M. 1973 *Nucl. Instrum. Meth.* **107**, 501–507.
Doniach, S. & Engelsberg, S. 1966 *Phys. Rev. Lett.* **17**, 750–753.
Glyde, H. R. & Khanna, F. C. 1977 *Can. J. Phys.* **55**, 1906–1923.
Glyde, H. R. & Khanna, F. C. 1980 *Can. J. Phys.* **58**, 343–350.
Hilton, P. A., Cowley, R. A., Stirling, W. G. & Scherm, R. 1978 *Z. Phys.* B **30**, 107–110.
Kitchens, T. A., Oversluizen, T., Passell, L. & Schermer, R. I. 1974 *Phys. Rev. Lett.* **32**, 791–794.
Kleb, R., Ostrowski, G. E., Price, D. L. & Rowe, J. M. 1973 *Nucl. Instrum. Meth.* **106**, 221–229.
Pines, D. 1966 In *Quantum fluids*, pp. 257–266. Amsterdam: North-Holland.
Price, D. & Sköld, K. 1970 *Nucl. Instrum. Meth.* **82**, 208–222.
Price, D. L. 1978 In *The physics of liquid and solid helium*, part 2, pp. 675–726. New York: John Wiley & Sons.
Scherm, R., Stirling, W. G., Woods, A. D. B., Cowley, R. A. & Coombs, G. I. 1974 *J. Phys.* C **7**, L341–345.
Sköld, K. 1968*a* *Bull. Am. phys. Soc.* (II), **13**, 467.
Sköld, K. 1968*b* *Nucl. Instrum. Meth.* **63**, 114–116.
Sköld, K. & Pelizzari, C. A. 1977 In *Quantum fluids and solids*, pp. 195–205. New York: Plenum.
Sköld, K. & Pelizzari, C. A. 1978*a* *J. Phys.* C **11**, L589–592.
Sköld, K. & Pelizzari, C. A. 1978*b* (Unpublished.)
Sköld, K., Pelizzari, C. A., Kleb, R. & Ostrowski, G. E. 1976 *Phys. Rev. Lett.* **37**, 842–845.
Sköld, K., Pelizzari, C. A., Kleb, R. & Ostrowski, G. E. 1980 (In preparation.)
Stirling, W. G., Scherm, R., Hilton, P. A. & Cowley, R. A. 1976 *J. Phys.* C **9**, 1643–1663.
Stirling, W. G., Scherm, R., Volino, F. & Cowley, R. A. 1975 In *Proceedings of the Fourteenth International Conference on Low Temperature Physics*, Otaniemi, Finland, pp. 76–79. Amsterdam: North-Holland.

PHILOSOPHICAL TRANSACTIONS OF THE ROYAL SOCIETY B BIOLOGICAL SCIENCES